5160 *Biochemistry* **2010,** *49,* 5160–5166
DOI: 10.1021/bi100626f

BIOCHEMISTRY
including biophysical chemistry & molecular biology
Article

Arginines 65 and 310 in Putidaredoxin Reductase Are Critical for Interaction with Putidaredoxin[†]

Irina F. Sevrioukova*[,‡] and Thomas L. Poulos[‡,§]

[‡]*Departments of Molecular Biology and Biochemistry,* [§]*Chemistry, and Pharmaceutical Sciences, University of California, Irvine, California 92697-3900*

Received April 23, 2010; Revised Manuscript Received May 24, 2010

ABSTRACT: In this study, we test the functional validity of the recently determined crystal structure of a covalently linked putidaredoxin reductase (Pdr)−putidaredoxin (Pdx) complex. The structure predicts several surface residues in Pdr as important for complex formation and/or electron transfer (ET). The R65A, R310A, R310E, K339A, N384A, K387A, and K409A mutants of Pdr have been prepared and characterized, and the mutational effects on the kinetics of Pdx reduction during single and steady-state turnover have been assessed. Replacement of Asp384 was found to have no effect on the Pdr−Pdx interaction. The K339A, K387A, and K409A substitutions moderately inhibited the binding affinity and reduction of Pdx, whereas the R65A and R310A mutations lowered the interprotein ET rate by 20−30-fold without perturbing the Pdx association step. The charge reversal on Arg310 had the most profound effect and decreased both the Pdr-to-Pdx ET and partner binding affinity by 100- and 8-fold, respectively. Our findings support the structural data and suggest that (i) the X-ray model is biologically relevant, (ii) arginines 65 and 310 are the key elements required for the formation of a productive ET complex with Pdx, (iii) the C-terminal lysine cluster assists in Pdx docking by fine-tuning Pdr−Pdx interactions to achieve the optimal geometry between the redox centers, and (iv) the basic surface residues in Pdr-like ferredoxin reductases not only define specificity for the redox partner but also may facilitate its dissociation.

In the camphor monooxygenase system from *Pseudomonas putida*, putidaredoxin reductase (Pdr)[1] catalyzes NADH-dependent reduction of a [2Fe-2S] ferredoxin, putidaredoxin (Pdx), which subsequently transfers electrons to the terminal oxygenase, cytochrome P450cam (P450cam). Pdr contains one tightly bound FAD whose midpoint redox potential changes from −369 to −230 mV upon NAD binding, which may provide the thermodynamic driving force that promotes electron transfer (ET) from NADH to Pdx in vivo (*1*). The NADH oxidation and Pdx reduction reactions catalyzed by Pdr are tightly coupled, with a turnover reaching 16000 min^{-1} (*2*). Formation of the Pdr−Pdx complex is guided by both ionic and nonionic interactions and steric complementarity (*3*−*12*). Several residues in Pdx, such as Tyr33, Asp38, Arg66, Glu72, and Cys73, were identified as being important for association with Pdr (*5*, *9*, *11*), whereas Asp38 and Cys39 were proposed to comprise an ET pathway to the metal center (*11*).

A breakthrough in understanding the mechanism of the Pdr−-Pdx pair was the determination of the X-ray structure of a covalent, fully functional complex between the partners (*13*). The crystallographic model provides a detailed view of the Pdr−Pdx interface, identifies interacting residues, suggests the shortest FAD-to-[2Fe-2S] ET route, and, importantly, agrees well with the previous experimental and theoretical results. This and a high degree of similarity between the Pdr−Pdx complex and other homologous redox complexes, such as the oxygenase-coupled ferredoxin reductase (BphA4)−Rieske-type ferredoxin (BphA3) complex from *Pseudomonas* sp. (*14*) and the bovine adrenodoxin reductase−adrenodoxin complex (*15*), allowed us to conclude that the crystallographic model closely resembles the ET complex formed between native Pdr and Pdx.

The crystallized Pdr−Pdx complex, however, has several features that are not present in the native complex. In addition to an artificially introduced $Lys409^{Pdr}$−$Glu72^{Pdx}$ cross-link, these include the C73S and C85S mutations in Pdx, a polyhistidine affinity tag in Pdr, and X-ray-induced photoreduction of the iron−sulfur cluster. The covalent link decreases the degree of motional freedom and, hence, may prevent the partners from reaching the optimal geometry. Residue 73 in Pdx is located at the edge of the crystallographic protein−protein interface (*13*) and was proven to regulate interaction with Pdr (*5*, *16*). The C-terminal polyhistidine peptide affects the redox properties of Pdr (*2*) and could perturb both association and ET to Pdx. Reduction of the metal cluster by synchrotron radiation, in turn, may induce conformational reorganization in the [2Fe-2S]-binding loop and surrounding residues (*17*), which could change the surface properties and, as a consequence, affinity for Pdr. Altogether, these factors raise the possibility that the Pdr−Pdx interface in the native complex may differ somewhat form that observed in the crystals.

[†]This study was supported by National Institutes of Health Grants GM67637 (I.F.S.) and GM33688 (T.L.P.).

*To whom correspondence should be addressed: Department of Molecular Biology and Biochemistry, 3205 McGaugh Hall, University of California, Irvine, CA 92697-3900. Telephone: (949) 824-1953. Fax: (949) 824-3280. E-mail: sevrioui@uci.edu.

[1]Abbreviations: Pdr, putidaredoxin reductase; Pdx, putidaredoxin; P450cam, camphor-hydroxylating cytochrome P450 from *P. putida*; BphA4 and BphA3, oxygenase-coupled ferredoxin reductase and Rieske-type ferredoxin from *Pseudomonas* sp., respectively; ET, electron transfer; WT, wild type; DCIP, 2,6-dichlorophenolindophenol; PuR, palustriredoxin reductase from *Rhodopseudomonas palustris*; PDB, Protein Data Bank.

 Published on Web 06/04/2010

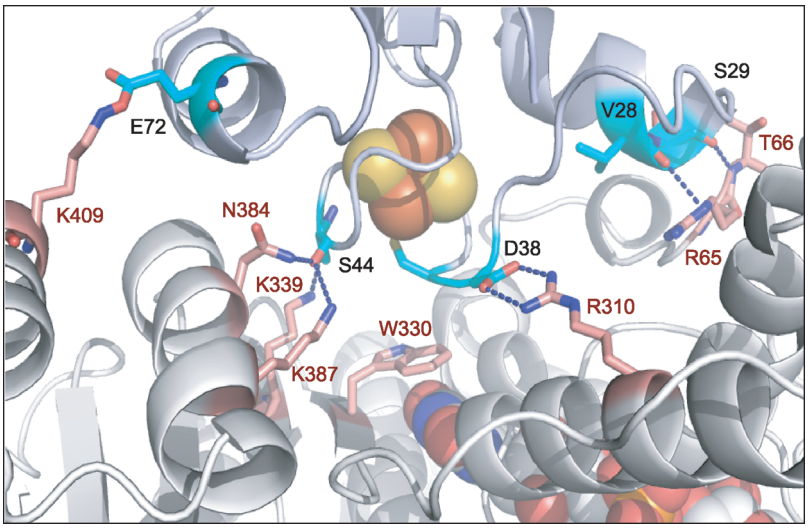

FIGURE 1: Protein−protein interface in the crystallographic Pdr−Pdx complex (*13*). Pdr is colored gray and pink and Pdx light blue and cyan. The FAD and [2Fe-2S] cofactors are in CPK representation. Only residues involved in hydrogen bonding and charge−charge interactions are shown. The $Lys409^{Pdr}$−$Glu72^{Pdx}$ salt bridge is chemically linked (*13*).

This study was undertaken with a dual goal: to experimentally test the functional relevance of the X-ray structure and to investigate structure−function relations in Pdr since no mutagenesis studies of the flavoenzyme have been performed thus far. In particular, we analyzed how substitutions of Arg65, Arg310, Lys339, Asn384, Lys387, and Lys409, the residues establishing hydrogen bonding or charge−charge interactions at the crystallographic complex interface (Figure 1), affect redox properties of tag-free Pdr as well as its interaction and ET to Pdx. The basic surface residues were found to modulate the redox potential of Pdr and interaction with small electron acceptor molecules, whereas the cluster of C-terminal lysines 339, 387, and 409 was identified as being important and arginines 65 and 310 as critical for establishing a productive ET complex with Pdx. Overall, our results strongly support the structural data and suggest that the crystallographic and native Pdr−Pdx complexes are highly similar.

EXPERIMENTAL PROCEDURES

Protein Preparation. The R65A, R310A, R310E, K339A, N384A, K387A, and K409A replacements in Pdr were introduced using the Stratagene QuikChange kit. Expression and purification of wild-type (WT) and mutant Pdr and Pdx were conducted as reported previously (*2*, *16*). The polyhistidine tag in Pdr was cleaved during overnight incubation with thrombin (2 units/mg, Sigma) in 50 mM phosphate (pH 8.0). Both undigested protein and the affinity tag were removed when the thrombin reaction mixture was passed through the Ni^{2+}-affinity column. Extinction coefficients of the Pdr mutants were determined in 100 mM phosphate buffer (pH 7.0) on the basis of the amount of FAD released upon SDS denaturation [ε_{450} = 11.3 mM^{-1} cm^{-1} (*18*)].

Spectral Measurements. Conventional spectroscopy was performed on a Cary 3 spectrophotometer. Stopped-flow kinetic measurements were taken under anaerobic conditions on an SX.18MV spectrophotometer (Applied Photophysics) in 50 mM phosphate (pH 7.5). Solutions were made anaerobic by repeated evacuating and flushing with prepurified argon and included an oxygen scrubbing system consisting of 5 mM glucose, 5 units/mL glucose oxidase, and 2 units/mL catalase. The kinetics of Pdr reduction with NADH was monitored at 454 nm and 4 °C. ET from Pdr to Pdx was followed at 507 nm, an isosbestic point for the reduced and oxidized Pdr, and 22 °C. Before being mixed with Pdx, Pdr was reduced with a 1.5-fold excess of NADH. Kinetic data were analyzed using IgorPro (WaveMetrics, Inc.). The limiting k_{obs} (k^{ET}) and K_d values were calculated from the hyperbolic fits to the k_{obs} versus Pdx concentration plots. Redox potentials of Pdr were determined spectrophotometrically according to Massey (*19*) in anaerobic solutions of xanthine-saturated 100 mM phosphate (pH 8.5) containing 20 μM protein, 2 μM benzyl viologen (E° = −359 mV), and catalytic amounts of xanthine oxidase (Sigma).

Redox Activity Assays. NADH-dependent reductase activities of Pdr toward 2,6-dichlorophenolindophenol (DCIP) and $K_3Fe(CN)_6$ were measured in 50 mM phosphate (pH 7.5) at 25 °C using an ε_{600} of 21 mM^{-1} cm^{-1} and an ε_{420} of 1.02 mM^{-1} cm^{-1}, respectively. The steady-state kinetics of cytochrome *c* reduction was followed in 5 mM phosphate (pH 7.5) at 25 °C and calculated using an ε_{550} of 21 mM^{-1} cm^{-1}. The rate of NADH consumption during camphor hydroxylation by the complete camphor monooxygenase system was determined at 25 °C and 340 nm (ε_{340} = 6.22 mM^{-1} cm^{-1}) in 20 mM phosphate (pH 7.5) containing 100 mM KCl, 0.5 μM WT or mutant Pdr, 5 μM Pdx, and 0.5 μM P450cam. The reaction was initiated with 0.3 mM NADH in the absence or presence of 0.5 mM camphor.

RESULTS AND DISCUSSION

Testing the Predicted ET Route. In the crystal structure of the Pdr−Pdx complex, the shortest ET path from FAD to [2Fe-2S] was predicted to proceed through $Trp330^{Pdr}$ and $Cys39^{Pdx}$ and require two through-space electron jumps (Figure 2). Taking into account the fact that elimination of the iron-ligating cysteines in ferredoxins severely perturbs the incorporation and redox properties of the metal cluster (*20*−*22*), we attempted to mutate only Trp330 in Pdr. Unfortunately, substitution of the tryptophan even with aromatic Phe and Tyr abolished Pdr expression. Since the indole ring of Trp330 shields the isoalloxazine group of FAD from solvent (Figure 1S of the Supporting Information), a decreased volume of the side chain at this position could significantly increase the level of solvation of the active site and interfere with folding and cofactor binding.

Rationale for the Surface Mutations in Pdr. The X-ray model can be evaluated also by modifying the surface properties of Pdr and assessing how it affects the binding affinity and ET to Pdx. The Pdr residues involved in specific interactions at the protein−protein interface include Arg310 and Lys409, forming salt bridges with Asp38 and Glu72 of Pdx, respectively, and Arg65, Thr66, Lys339, Asn384, and Lys387, establishing H-bonds with Val28, Ser29, and Ser44 of Pdx (Figure 1) (*13*). Since Thr66 provides the main chain for H-bond formation, it was not included in this study. Arg65, Arg310, Lys339, Asn384, Lys387, and Lys409, in turn, were replaced with Ala. Because of the central location of the strong bidentate $Arg310^{Pdr}$−$Asp38^{Pdx}$ salt bridge, an R310E mutation was also prepared in anticipation that the charge reversal should have a stronger effect on the Pdr−Pdx interaction. Finally, although interaction between Pdr K409A and Pdx has been investigated by the cross-linking technique (*12*), we included this Pdr variant in the kinetic study to analyze the mutational effect on the Pdr-to-Pdx ET.

Characterization of the Pdr Mutants. Similar to WT, all Pdr mutants were expressed in *Escherichia coli* as holoproteins and had absorbance maxima at 271−272, 377−378, and 453−454 nm (Figure 2S of the Supporting Information and Table 1). Although FAD incorporation was seemingly unperturbed, the surface mutations did change the flavin environment, as evidenced by the difference in the flavin extinction coefficients and redox potentials (Table 1). Furthermore, all Pdr variants except N384A reacted with NADH somewhat slower than WT while having similar K_d values for the reductant (Table 1). These observations suggest that the basic residues may elevate the flavin redox potential to promote ET from NADH.

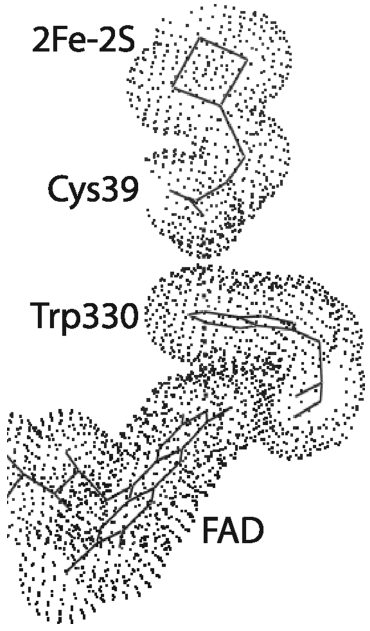

FIGURE 2: Electron transfer pathway from FAD to [2Fe-2S] predicted by HARLEM (*26*) based on the crystal structure of the covalent Pdr−Pdx complex (*13*). The route includes two through-space (3.6 Å) electron jumps: FAD to $Trp330^{Pdr}$ and $Trp330^{Pdr}$ to $Cys39^{Pdx}$.

The mutations also affected the electron donating ability of Pdr. The reductase activities of the R310A, N384A, K384A, and K409A variants toward one- and two-electron-accepting $K_3Fe(CN)_6$ and DCIP, respectively, were unchanged or increased, whereas the corresponding activities of Pdr R65A, R310E, and K339A were decreased by ∼20−50% (Table 2). The latter three mutations, as well as R310A, significantly weakened ET to cytochrome *c*. The K387A replacement had a moderate inhibitory effect on cytochrome *c* reduction, while the N384A substitution increased hemoprotein reduction rate by 40%. Notable changes in the turnover and K_d for DCIP and $K_3Fe(CN)_6$ caused by the Arg65, Arg310, and Lys339 mutations suggest that these basic residues may regulate access of the acceptor molecules to the active site of Pdr.

Effect of Pdr Mutations on the Turnover of P450cam Monooxygenase. We next determined the effect of Pdr mutations on the turnover of the reconstituted P450cam monooxygenase system by monitoring camphor-dependent NADH consumption at saturating levels of Pdx (1:10:1 Pdr:Pdx:P450cam ratio). Our experiments showed that the R65A, R310A, and R310E mutations in Pdr virtually abolished NADH oxidation (∼0.2−0.3% of WT oxidation); removal of the Lys339, -387, and -409 side chains decreased the turnover number by 80, 90, and 50%, respectively, while the N384A replacement had no effect (Figure 3).

When the E72A variant of Pdx was used in the assay, there was a further 15−30% decrease in the rate of turnover of WT, K339A, and N384A Pdr, and a smaller decline for the K387A and K409A mutants [∼3−8% (Figure 3)]. Since the negative charge on $Glu72^{Pdx}$ does not contribute to the Pdx−P450cam interaction (*9*) and reduction of Pdr with NADH does not limit the overall reaction, the observed inhibitory effect of the E72A mutation may be attributed to the perturbed Pdr−Pdx association, possibly, due to the lack of formation of the $Lys409^{Pdr}$–$Glu72^{Pdx}$ salt link (*12*).

Effect of Pdr Mutations on the FAD-to-[2Fe-2S] ET. To confirm that the inhibitory effect of Pdr mutations on the camphor-dependent NADH consumption by P450cam monooxygenase is due to perturbed Pdr−Pdx interaction, we measured kinetic parameters for the FAD-to-[2Fe-2S] ET reaction by mixing prereduced Pdr with various concentrations of oxidized Pdx in a stopped-flow apparatus. Although the rate of Pdx

Table 1: Spectral and Redox Properties of the Pdr Mutants

	λ_{max} (nm)	ε_{454} (mM^{-1} cm^{-1})	$E^{o a}$ (mV)	$k^{ET}{}_{NADH}{}^{b}$ (s^{-1})	$K_d{}^{NADH}$ (μM)
WT	454, 378, 272	11.0 ± 0.2	−342 ± 4	806 ± 9	81 ± 4
R65A	454, 378, 272	11.3 ± 0.3	−356 ± 5	754 ± 23	38 ± 3
R310A	453, 377, 272	11.8 ± 0.4	−367 ± 3	729 ± 9	34 ± 2
R310E	453, 377, 272	10.8 ± 0.2	−367 ± 4	720 ± 13	81 ± 6
K339A	454, 378, 272	10.8 ± 0.3	−347 ± 2	650 ± 23	70 ± 6
N384A	454, 378, 271	10.7 ± 0.2	−343 ± 3	820 ± 20	87 ± 7
K387A	454, 378, 271	10.9 ± 0.2	−357 ± 2	780 ± 22	97 ± 7
K409A	454, 378, 271	10.9 ± 0.3	−365 ± 2	800 ± 28	113 ± 8

[a]Determined at pH 8.5. [b]Measured at 4 °C.

Table 2: Effect of Pdr Mutations on the Redox Activity toward Small Electron Acceptors and Cytochrome *c*

	DCIP			$K_3Fe(CN)_6$			cytochrome *c*
	turnover (min^{-1})	K_M^{DCIP} (μM)	K_M^{NADH} (μM)	turnover (min^{-1})	$K_M^{K_3Fe(CN)_6}$ (μM)	K_M^{NADH} (μM)	k^{ET} (M^{-1} min^{-1})
WT	23100 ± 600 (100%)	97 ± 4	27 ± 3	58900 ± 4900 (100%)	40 ± 4	38 ± 3	$(2.2 \pm 0.1) \times 10^5$ (100%)
R65A	12200 ± 300 (53%)	29 ± 2	17 ± 2	33600 ± 1500 (57%)	50 ± 3	34 ± 5	$(8.0 \pm 0.2) \times 10^4$ (36%)
R310A	37000 ± 900 (160%)	125 ± 11	18 ± 3	89100 ± 3270 (150%)	143 ± 8	36 ± 4	$(1.2 \pm 0.1) \times 10^5$ (55%)
R310E	17000 ± 800 (74%)	200 ± 26	37 ± 4	47400 ± 3270 (80%)	40 ± 5	37 ± 5	$(1.1 \pm 0.3) \times 10^5$ (50%)
K339A	17300 ± 750 (75%)	125 ± 4	22 ± 3	32600 ± 1630 (72%)	45 ± 6	25 ± 3	$(7.0 \pm 0.2) \times 10^4$ (32%)
N384A	21500 ± 400 (93%)	83 ± 2	50 ± 6	53900 ± 3800 (120%)	43 ± 4	50 ± 6	$(3.1 \pm 0.1) \times 10^5$ (141%)
K387A	24500 ± 850 (106%)	83 ± 3	42 ± 2	46300 ± 1630 (103%)	44 ± 3	36 ± 4	$(1.6 \pm 0.1) \times 10^5$ (73%)
K409A	22600 ± 900 (98%)	91 ± 6	31 ± 2	45300 ± 3800 (101%)	36 ± 4	29 ± 4	$(2.5 \pm 0.2) \times 10^5$ (114%)

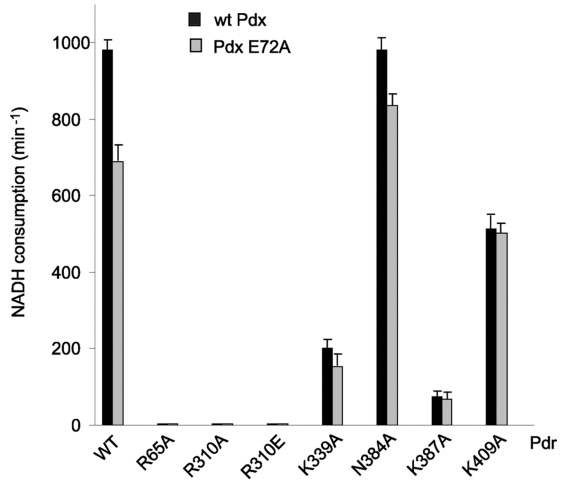

FIGURE 3: Effect of Pdr mutations on NADH consumption during turnover of the camphor monooxygenase system (1:10:1 Pdr:Pdx:P450cam ratio). The camphor-dependent NADH oxidation rates were measured in the presence of the WT (black bars) or E72A Pdx (gray bars) as described in Experimental Procedures.

reduction may not reflect the true FAD-to-[2Fe-2S] electron transfer process due to significant conformational reorganization in Pdx (*17*) and possibly in Pdr, for the sake of simplicity we will use terms "ET rate" and "k^{ET}" for the observed and limiting values of the rate constant, respectively. The single-turnover ET measurements correlated well with the steady-state kinetics. As seen in Figure 4a and Table 3, the N384A replacement had no effect on the association and reduction of Pdx, meaning that the asparagine side chain does not contribute to redox partner recognition. The K339A, K387A, and K409A replacements had a moderate inhibitory effect on the Pdr-to-Pdx ET, with only K387A perturbing the redox partner binding (i.e., higher K_d). Given that none of these three residues is predicted by the crystal structure to comprise an ET path to Pdx, we hypothesize that this C-terminal lysine cluster plays only a moderate role in redox partner recognition by fine-tuning interactions at the interface.

Removal of the positively charged side chains at positions 65 and 310 had a more profound effect on interprotein ET and decreased the electron transfer rate by 20−30-fold without significantly affecting the Pdr−Pdx complex affinity. Although the lack of an effect of the R310A mutation on K_d may seem unusual, it can be explained on the basis of the crystal structure and our previous kinetic study, showing a biphasic dependence of k_{obs} for the Pdr-to-Pdx ET on ionic strength, reaching a maximum at μ = 0.3 (*10*). This suggests that electrostatic attraction and hydrophobic interactions between Pdr and Pdx need to be balanced for optimal ET. In this study, interprotein ET measurements were conducted at a moderately low ionic strength (μ = 0.1), which may mask the charge elimination effects because of suboptimal conditions for formation of the Pdr−Pdx complex. Also, positioned nearby, Lys319, Arg322, and Lys387 could compensate for the loss of a positive charge at position 310 and assist in the docking of Pdx to the R310A mutant. Replacement of Arg310 with a long-chain acidic residue, on the other hand, drastically changes the surface properties and could lead to electrostatic repulsion during association with Pdx. Indeed, kinetic measurements show that the charge reversal on Arg310 not only decreases the ET rates by 2 orders of magnitude but also weakens the binding ability of Pdx by ~8-fold (Figure 4a,b and Table 3). Since Arg310 is quite remote from the isoalloxazine ring, the redox moiety of FAD (Figure 3S of the Supporting Information), its direct participation in Pdx reduction is unlikely. Instead, this basic residue could regulate ET indirectly by assisting docking and optimally orienting Pdx via formation of a salt bridge with $Asp38^{Pdx}$. As found previously, comprising the metal-binding loop, Asp38 is critical for establishing a productive ET complex with Pdr and mediation of Pdr-to-Pdx ET, where both the negative charge and the side-chain length of the residue are thought to play a role (*7*, *11*, *12*). Thus, in accord with the notion that electrostatic interactions involving charged groups at or near the ET site strongly influence long-range ET reactions (*23*), we identified the $Arg310^{Pdr}$−$Asp38^{Pdx}$ charge−charge pair as an important modulator of interprotein ET in the Pdr−Pdx couple. Since the D38N substitution in Pdx significantly affects the kinetic reversibility of [2Fe-2S] cluster oxidation and reduction (*11*), it is possible that, in addition to guiding dynamic interactions and conformational geometry within the complex with Pdr, the carboxyl group in Asp38 can change the protonation state and couple electron and proton transfer. In this regard, further mutagenesis studies and investigation into how Pdr-to-Pdx ET is affected by pH would help us gain more detailed insights into the roles played by individual amino acids and the reaction mechanism, in general.

While the critical role of Arg310 in formation of the Pdr−Pdx complex can be easily explained on the basis of the crystal structure (*13*), a strong inhibiting effect of the R65A mutation is somewhat puzzling. One possible explanation is that, in addition to establishing specific polar interactions (Figure 1), peripherally located Arg65 may prevent Pdx from sliding deeper into the active site of Pdr, which could not only help to maintain the complex geometry but also facilitate redox partner dissociation. Superposition of the Pdx-free and Pdx-bound structures of Pdr (Figure 5) shows that, contrary to other mutated residues that remain in nearly the same conformation, the side chain of

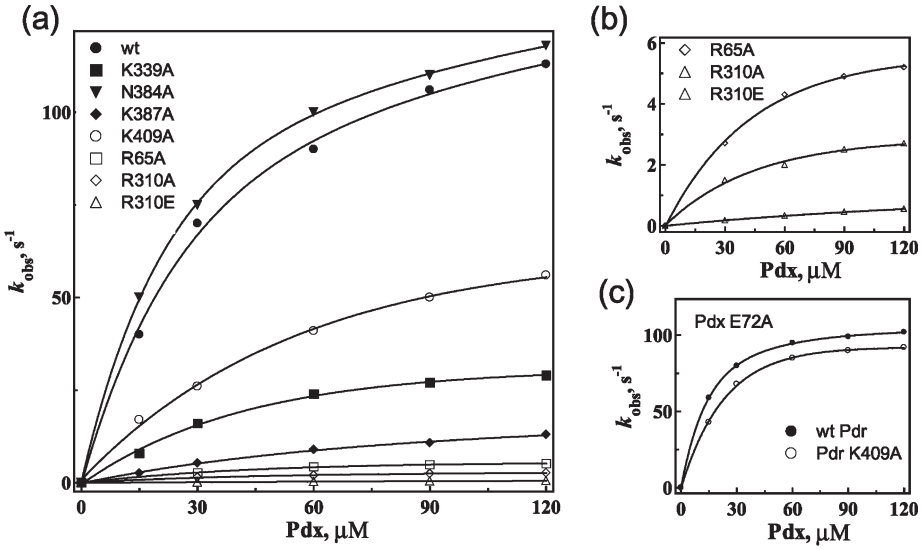

FIGURE 4: (a) Effect of Pdr mutations on the kinetics of Pdx reduction. The FAD-to-[2Fe-2S] ET was followed under anaerobic conditions at 507 nm and ambient temperatures. The reaction mixture contained 30 μM wild-type or mutant Pdr and various concentrations of Pdx. Kinetic parameters obtained from the hyperbolic fits (shown as solid lines) are given in Table 3. (b) Zoomed in view of the k_{obs} vs [Pdx] plots for the R65A and R310A and -E mutants. (c) Plots of the observed ET rate constants vs [Pdx] for the reactions between Pdx E72A and WT or K409A Pdr.

Table 3: Effect of Pdr Mutations on the Pdr-to-Pdx ET

Pdr	k^{ET} (s^{-1})	K_d (μM)
	WT Pdx	
WT	148 ± 5 (100%)	37 ± 4
R65A	7.5 ± 0.5 (5%)	49 ± 8
R310A	3.8 ± 0.2 (3%)	48 ± 7
R310E	1.9 ± 0.2 (1%)	284 ± 37
K339A	43 ± 3 (29%)	52 ± 9
N384A	145 ± 1 (98%)	28 ± 1
K387A	25 ± 2 (17%)	116 ± 16
K409A	87 ± 3 (59%)	68 ± 5
	E72A Pdx	
WT	114 ± 1 (77%)	13 ± 1
K409A	105 ± 4 (79%)	21 ± 3

Arg65 reorients to direct the guanidine group toward the $Asp18^{Pdr}$ carboxyl group and form H-bonds with the carbonyl oxygens of $Leu64^{Pdr}$ and $Val28^{Pdx}$. With the Phe21 ring lying underneath, this Arg65 conformation creates a rigid buffer zone complementary to the Pdx surface that may act as a "stopper" regulating how deeply Pdx can penetrate into the active site of Pdr. If this were the case, replacing Arg65 with Ala would not only disrupt polar interactions but also "soften" the buffer zone, leading to the displacement and misorientation of the redox partners.

Finally, comparative kinetics of Pdx E72A reduction by WT and K409A Pdr (Figure 4c and Table 3) suggests that the $Lys409^{Pdr}$–$Glu72^{Pdx}$ salt link may indeed be established between the native proteins. Again, taking into account the fact that the affinity of both WT and K409A Pdr for Pdx E72A is higher than for the native iron–sulfur protein, we can attribute the observed decrease in the ET rates to the redox partners' misalignment and distorted complex geometry rather than to changes in the ET step.

Conservation of Key Residues in the Homologous Flavoproteins. Structural comparison of Pdr and its two closely related homologues, BphA4 (*24*) and palustriredoxin reductase (PuR) from *Rhodopseudomonas palustris* (*25*), revealed that among five arginines and lysines identified by this study as being important for Pdr–Pdx interaction only one basic residue at position 387 (Pdr numbering) is conserved (Figure 6a). Three other residues, Arg65, Arg310, and Lys409, are present in PuR but replaced with acidic or hydrophobic amino acids in BphA4. Another element common for Pdr and PuR is an $\alpha 2_2$-helix, connected to Arg65 via threonine and proline, respectively (Figure 6b). Although PuR lacks a bulky residue corresponding to Phe21, the proline-mediated connection may provide the conformational rigidity in this area necessary for controlling association and dissociation of the redox partner.

A high degree of surface similarity in Pdr and PuR predicts that the latter may be a suitable redox partner for Pdx. Indeed, it has recently been shown that PuR catalyzes Pdx reduction during steady-state turnover at low ionic strengths more efficiently than Pdr (*25*). At higher salt concentrations, however, ET between the Pdr–Pdx pair becomes more efficient, which confirms the importance of hydrophobic forces for Pdr–Pdx association (*10*) and suggests that Pdr may be better suited for reducing Pdx under physiological conditions. Another interesting finding was the fact that substitution of Lys328 in PuR (Gly337 in Pdr) with Gly decreased K_M for Pdx and k_{cat} by 4–5-fold (*25*). This suggests that the long-chain basic residues on the surface of Pdr-like ferredoxin reductases not only provide favorable electrostatic interactions but also may prevent their redox partners from penetrating too deeply into the active site and facilitate the dissociation step.

In conclusion, our study provides the first insight into structure–function relationships in Pdr with respect to electron transfer to Pdx. We have found that the surface residues Arg65, Arg310, Lys339, Lys387, and Lys409 modulate the redox potential and interaction of Pdr with small electron acceptor molecules. Most importantly, we show that the C-terminal Lys339, -387, and -409 cluster is important and Arg65 and -310 are critical for establishing a productive ET complex with Pdx. Good correlation between the kinetic and structural results allows us to conclude that the crystallographic Pdr–Pdx complex

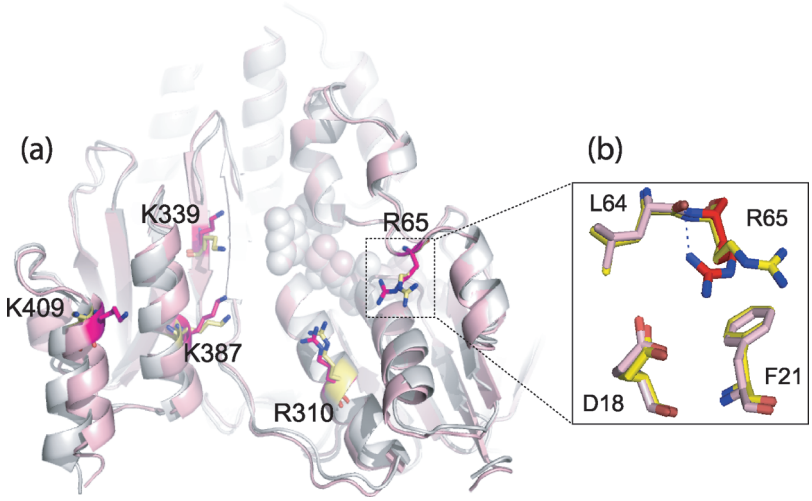

FIGURE 5: (a) Least-squares superposition of the crystal structures of intact [gray and yellow; PDB entry 1Q1R (*13*)] and Pdx-bound Pdr [pink and magenta; PDB entry 3LB8 (*13*, *27*)]. Only the side chains of mutated resides are displayed. (b) Conformational reorganization in Arg65. Upon Pdx binding, the guanidine group flips by 180° to orient toward Asp18 and establish an H-bond with the Leu64 carbonyl oxygen.

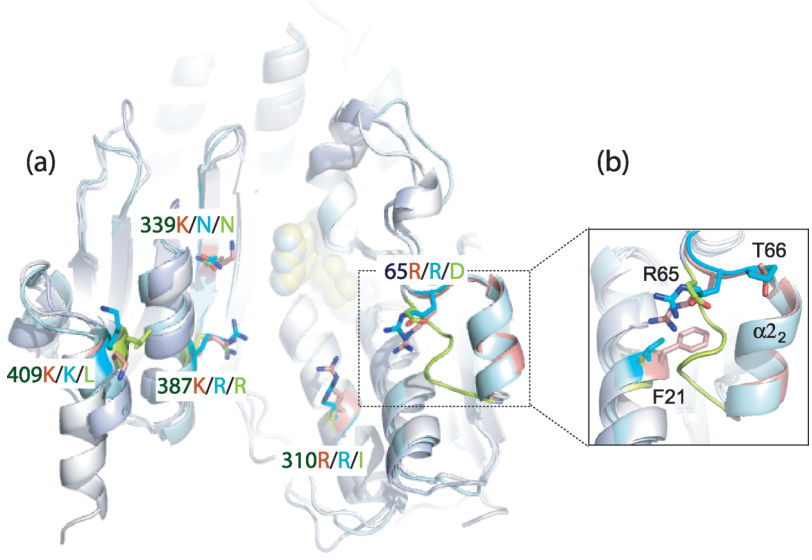

FIGURE 6: (a) Structural comparison of Pdr (gray and red) and homologous ferredoxin reductases, PuR (light and deep cyan) and BphA4 (light blue and green) [PDB entries 1Q1R, 3FG2, and 1D7Y, respectively (*24*, *25*, *27*)]. Only the side chains of residues corresponding to those involved in Pdx binding are displayed. (b) Similarity of the Pdr and PuR structures in the vicinity of Arg65. PuR is missing a Phe at position 21 but has a proline connecting the $\alpha 2_2$-helix to Arg65 (Pdr numbering), which may increase the rigidity of the area likely involved in the association and dissociation of the redox partner.

is biologically relevant and can serve as a useful model for the natural noncovalent ET complex. Comparative structural analysis of the ferredoxin reductases homologous to Pdr, in turn, suggests that, having evolved together with the terminal oxygenase, each flavoprotein acquired structural elements required for maintaining ET activity at a level that precludes accumulation of the reduced partner and futile loss of electrons.

SUPPORTING INFORMATION AVAILABLE

A view of the semitransparent surface above the active site of Pdr with the side chains of residues shielding the isoalloxazine ring of FAD displayed (Figure 1S), absorbance spectra of Pdr mutants (Figure 2S), and protein−protein interface in the crystallographic Pdr−Pdx complex showing positioning of the $Arg310^{Pdr}$–$Asp38^{Pdx}$ salt bridge relative to FAD (Figure 3S). This material is available free of charge via the Internet at http://pubs.acs.org.

REFERENCES

1. Reipa, V., Holden, M. J., and Vilker, V. L. (2007) Association and redox properties of the putidaredoxin reductase-nicotinamide adenine dinucleotide complex. *Biochemistry 46*, 13235–13244.
2. Sevrioukova, I. F., and Poulos, T. L. (2002) Putidaredoxin reductase: A new function for an old protein. *J. Biol. Chem. 277*, 25831–25839.
3. Geren, L., Tuls, J., O'Brien, P., Millett, F., and Peterson, J. A. (1986) The involvement of carboxylate groups of putidaredoxin in the reaction with putidaredoxin reductase. *J. Biol. Chem. 261*, 15491–15495.
4. Roome, P. W., and Peterson, J. A. (1988) The oxidation of reduced putidaredoxin reductase by oxidized putidaredoxin. *Arch. Biochem. Biophys. 266*, 41–50.
5. Holden, M., Mayhew, M., Bunk, D., Roitberg, A., and Vilker, V. (1997) Probing the interactions of putidaredoxin with redox partners in camphor P450 5-monooxygenase by mutagenesis of surface residues. *J. Biol. Chem. 272*, 21720–21725.
6. Aoki, M., Ishimori, K., Fukada, H., Takahashi, K., and Morishima, I. (1998) Isothermal titration calorimetric studies on the associations of putidaredoxin to NADH-putidaredoxin reductase and P450cam. *Biochim. Biophys. Acta 1384*, 180–188.

7. Aoki, M., Ishimori, K., and Morishima, I. (1998) Roles of negatively charged surface residues of putidaredoxin in interactions with redox partners in P450cam monooxygenase system. *Biochim. Biophys. Acta 1386*, 157–167.
8. Aoki, M., Ishimori, K., and Morishima, I. (1998) NMR studies of putidaredoxin: Associations of putidaredoxin with NADH-putidaredoxin reductase and cytochrome P450cam. *Biochim. Biophys. Acta 1386*, 168–178.
9. Aoki, M., Ishimori, K., Morishima, I., and Wada, Y. (1998) Roles of valine-98 and glutamic acid-72 of putidaredoxin in the electron-transfer complexes with NADH-putidaredoxin reductase and P450cam. *Inorg. Chim. Acta 272*, 80–88.
10. Sevrioukova, I. F., Hazzard, J. T., Tollin, G., and Poulos, T. L. (2001) Laser flash induced electron transfer in P450cam monooxygenase: Putidaredoxin reductase−putidaredoxin interaction. *Biochemistry 40*, 10592–10600.
11. Kuznetsov, V. Y., Blair, E., Farmer, P. J., Poulos, T. L., Pifferitti, A., and Sevrioukova, I. F. (2005) The putidaredoxin reductase-putidaredoxin electron transfer complex: Theoretical and experimental studies. *J. Biol. Chem. 280*, 16135–16142.
12. Churbanova, I. Y., Poulos, T. L., and Sevrioukova, I. F. (2010) Production and characterization of a functional putidaredoxin reductase-putidaredoxin covalent complex. *Biochemistry 49*, 58–67.
13. Sevrioukova, I. F., Poulos, T. L., and Churbanova, I. Y. (2010) Crystal structure of the putidaredoxin reductase-putidaredoxin electron transfer complex. *J. Biol. Chem. 285*, 13616–13620.
14. Senda, M., Kishigami, S., Kimura, S., Fukuda, M., Ishida, T., and Senda, T. (2007) Molecular mechanism of the redox-dependent interaction between NADH-dependent ferredoxin reductase and Rieske-type [2Fe-2S] ferredoxin. *J. Mol. Biol. 373*, 382–400.
15. Muller, J. J., Lapko, A., Bourenkov, G., Ruckpaul, K., and Heinemann, U. (2001) Adrenodoxin reductase−adrenodoxin complex structure suggests electron transfer path in steroid biosynthesis. *J. Biol. Chem. 276*, 2786–2789.
16. Sevrioukova, I. F., Garcia, C., Li, H., Bhaskar, B., and Poulos, T. L. (2003) Crystal structure of putidaredoxin, the [2Fe-2S] component of the P450cam monooxygenase system from *Pseudomonas putida*. *J. Mol. Biol. 333*, 377–392.
17. Sevrioukova, I. F. (2005) Redox-dependent structural reorganization in putidaredoxin, a vertebrate-type [2Fe-2S] ferredoxin from *Pseudomonas putida*. *J. Mol. Biol. 347*, 607–621.
18. Prongay, A. J., Engelke, D. R., and Williams, C. H., Jr. (1989) Characterization of two active site mutations of thioredoxin reductase from *Escherichia coli*. *J. Biol. Chem. 264*, 2656–2664.
19. Massey, V. (1991) A simple method for the determination of redox potentials. In Flavins and Flavoproteins (Curti, B., Zanetti, G., and Ronchi, S., Eds.) pp 581−584, Walter de Gruyter, Como, Italy.
20. Cupp, J. R., and Vickery, L. E. (1988) Identification of free and $[Fe_2\text{-}S_2]$-bound cysteine residues of adrenodoxin. *J. Biol. Chem. 263*, 17418–17421.
21. Hurley, J. K., Weber-Main, A. M., Hodges, A. E., Stankovich, M. T., Benning, M. M., Holden, H. M., Cheng, H., Xia, B., Markley, J. L., Genzor, C., Gomez-Moreno, C., Hafezi, R., and Tollin, G. (1997) Iron-sulfur cluster cysteine-to-serine mutants of *Anabaena* [2Fe-2S] ferredoxin exhibit unexpected redox properties and are competent in electron transfer to ferredoxin:$NADP^+$ reductase. *Biochemistry 36*, 15109–15117.
22. Yeh, A. P., Chatelet, C., Soltis, S. M., Kuhn, P., Meyer, J., and Rees, D. C. (2000) Structure of a thioredoxin-like [2Fe-2S] ferredoxin from *Aquifex aeolicus*. *J. Mol. Biol. 300*, 587–595.
23. Tollin, G., Meyer, T. E., and Cusanovich, M. A. (1986) Elucidation of the factors which determine reaction-rate constants and biological specificity for electron-transfer proteins. *Biochim. Biophys. Acta 853*, 29–41.
24. Senda, T., Yamada, T., Sakurai, N., Kubota, M., Nashizaki, T., Masai, T., Fukuda, M., and Mitsui, Y. (2000) Crystal structure of NADH-dependent ferredoxin reductase component in biphenyl dioxygenase. *J. Mol. Biol. 304*, 397–410.
25. Xu, F., Bell, S. G., Peng, Y., Johnson, E. O., Bartlam, M., Rao, Z., and Wong, L. L. (2009) Crystal structure of a ferredoxin reductase for the CYP-199A2 system from *Rhodopseudomonas palustris*. *Proteins 77*, 867–880.
26. Kurnikov, I. V. (2000) Harlem molecular modeling package, version 1.0, Department of Chemistry, University of Pittsburgh, Pittsburgh, PA.
27. Sevrioukova, I. F., Li, H., and Poulos, T. L. (2004) Crystal structure of putidaredoxin reductase from *Pseudomonas putida*, the final structural component of the cytochrome P450cam monooxygenase. *J. Mol. Biol. 336*, 889–902.